



**Karolinska
Institutet**

Karolinska Institutet

<http://openarchive.ki.se>

This is a Peer Reviewed Accepted version of the following article, accepted for publication in Journal of Applied Physiology.

2019-09-03

Cardiac remodeling in aortic and mitral valve disease : a simulation study with clinical validation

Maksuti, Elira; Westerhof, Berend; Ugander, Martin; Donker, Dirk; Carlsson, Marcus; Broomé, Michael

J Appl Physiol. 2019 May 1;126(5):1377-1389.

Cambridge University Press

<http://doi.org/10.1152/jappphysiol.00791.2018>

<http://hdl.handle.net/10616/46844>

If not otherwise stated by the Publisher's Terms and conditions, the manuscript is deposited under the terms of the Creative Commons Attribution-NonCommercial-NoDerivatives License (<http://creativecommons.org/licenses/by-nc-nd/4.0/>), which permits non-commercial re-use, distribution, and reproduction in any medium, provided the original work is properly cited, and is not altered, transformed, or built upon in any way.



**Karolinska
Institutet**

This is an author produced version of a paper published in

Journal of Applied Physiology

This paper has been peer-reviewed, but does not include the final publisher proof-corrections or journal pagination.

Citation for the published paper:

**Maksuti E, Westerhof BE, Ugander M, Donker DW,
Carlsson M, Broomé M.
Cardiac remodeling in aortic and mitral valve disease: a
simulation study with clinical validation.
J Appl Physiol. 2019 May 1;126(5):1377-1389.**

URL: **<http://doi.org/10.1152/japplphysiol.00791.2018>**

Access to the published version may
require subscription.

Published with permission from:
American Physiological Society

Cardiac Remodeling in Aortic and Mitral Valve Disease – a Simulation Study with Clinical Validation

Short title: Cardiac Remodeling in Left-sided Valvular Disease

Elira Maksuti¹, Berend E. Westerhof², Martin Ugander³,
Dirk W. Donker⁴, Marcus Carlsson⁵, Michael Broomé^{1,6*}

¹ECMO Department, Karolinska University Hospital, Stockholm, Sweden

²Amsterdam UMC, Vrije Universiteit Amsterdam, Pulmonary Medicine, Amsterdam
Cardiovascular Sciences, Amsterdam, the Netherlands

³Department of Clinical Physiology, Karolinska Institutet, and Karolinska University
Hospital, Stockholm, Sweden

⁴Department of Intensive Care Medicine, University Medical Center Utrecht, Utrecht
University, The Netherlands

⁵Department of Clinical Sciences Lund, Clinical Physiology, Lund University, Skane
University Hospital, Lund, Sweden

⁶Anesthesia and Intensive Care, Dept. of Physiology and Pharmacology, Karolinska Institutet,
Stockholm, Sweden

Author contributions:

Conceived and designed the experiments: EM, MB. Performed the experiments: EM, MB.
Analyzed the data: All authors. Wrote initial draft: EM, MB. Further contributed to the
manuscript: BEW, MU, DWD, MC. Reviewed the manuscript: All authors.

*Corresponding author

Michael Broomé, MD, PhD

ECMO Department

Karolinska University Hospital

Stockholm, Sweden

E-mail: michael.broome@ki.se

Abstract

Background. Remodeling is an important long-term determinant of cardiac function throughout the progression of heart disease. Numerous biomolecular pathways for mechanosensing and transduction are involved. However, we hypothesize that biomechanical factors alone can explain changes in myocardial volume and chamber size in valve disease.

Methods. A validated model of the human vasculature and the four cardiac chambers was used to simulate aortic stenosis, mitral regurgitation and aortic regurgitation. Remodeling was simulated with adaptive feedback preserving myocardial fiber stress and wall shear stress in all four cardiac chambers. Briefly, the model used myocardial fiber stress to determine wall thickness and cardiac chamber wall shear stress to determine chamber volume.

Results. Aortic stenosis resulted in the development of concentric left ventricular hypertrophy. Aortic and mitral regurgitation resulted in eccentric remodeling and eccentric hypertrophy, with more pronounced hypertrophy for aortic regurgitation. Comparisons with published clinical data showed the same direction and similar magnitudes of changes in end-diastolic volume index and left ventricular diameters. Changes in myocardial wall volume and wall thickness were within a realistic range both in stenotic and regurgitant valvular disease.

Conclusions. Simulations of remodeling in left-sided valvular disease support, in both a qualitative and quantitative manner, that left ventricular chamber size and hypertrophy are primarily determined by preservation of wall shear stress and myocardial fiber stress.

Key words: Cardiac remodeling, Hypertrophy, Valvular disease, Wall shear stress, Myofiber stress, Simulations

New & Noteworthy

Cardiovascular simulations with adaptive feedback that normalizes wall shear stress and fiber stress in the cardiac chambers could predict – in a quantitative and qualitative manner – remodeling patterns seen in patients with left-sided valvular disease. This highlights how mechanical stress remains a fundamental aspect of cardiac remodeling. This *in silico* study validated with clinical data paves the way for future patient-specific predictions of remodeling in valvular disease.

Introduction

The concept of cardiac remodeling was originally coined to describe structural changes in the left ventricle after myocardial infarction, and is currently used in a broader context, referring to the heart's plasticity in general (5, 9, 20). Over the last decades, it has been considered of paramount importance to understand cardiac disease processes that manifest as changes in size, shape, structure and function of the myocardium. The remodeling process has been viewed both as a beneficial, adaptive response that counteracts the negative effects of disease (40) and as detrimental maladaptation causing organ failure and death (9, 12, 23, 49). One of the primary elements in cardiac remodeling is the response to biomechanical stresses (38), although neurohumoral factors, ion channels and cell-cell interactions may also contribute to intracellular signaling cascades that ultimately result in altered myocardial composition and cellular changes (20).

The cardiomyocyte has the capability to elongate by adding new sarcomeres in series as well as to increase its radius by adding sarcomeres in parallel as a response to mechanical stress (48). Left ventricular hypertrophy is a primary element of this structural remodeling process, and occurs both due to cellular growth and alterations of the extracellular matrix (9, 12, 40). Advances in cardiac magnetic resonance imaging now allow to measure and distinguish between cellular and matrix volume, and a recent study has shown that most cases of pathological ventricular hypertrophy result from a proportional increase in both cellular and matrix components (46).

In order to unravel the nature of the cardiac phenotype, simulations of hemodynamics based on established and validated physical laws are powerful tools to test mechanistic hypotheses within the cardiovascular system. The main driving mechanisms of mechanical adaptation to changing loading conditions need to be identified. So far, it has been postulated, that fiber stress (σ_f) plays an important role in cardiac remodeling and in particular as a determinant of wall thickness (18). Additionally, increased wall shear stress (σ_{wss}) has been suggested to cause vessel dilation in vascular remodeling (24, 36, 50), and we propose that it has a comparable effect in cardiac remodeling, where volume loading (increasing σ_{wss}) is known to cause dilatation in a way similar to vessel dilatation in response to increasing flow (26, 43). σ_{wss} can be described as the tangential frictional force between blood flow and the endothelium/endocardium. Based on these considerations, we hypothesize that preserving mean σ_f and mean σ_{wss} are the major biomechanical drivers of cardiac remodeling. Specifically, we assume σ_{wss} to be the major determinant of chamber size and σ_f the major factor responsible for changes in wall thickness

and myocardial volume. The aim of this study was to assess the validity of these hypotheses by comparing computer simulations with clinical imaging data in the three most common valve diseases (11, 28), i.e. in aortic stenosis, mitral regurgitation and aortic regurgitation, where early detection and appropriate timing of surgical intervention are of great clinical importance (21, 28).

Methods

A closed-loop real-time cardiovascular simulation model of the cardiovascular system previously developed and validated was used as simulation platform for this study (7, 8, 13). The model was expanded to include real-time calculations of σ_f and σ_{wss} to allow the implementation of adaptive remodeling rules.

Modeling assumptions

The following sections explain the geometrical assumptions made for the four cardiac chambers and the two adaptation rules implemented to simulate the cardiac remodeling process.

Chambers' geometry

Cardiac chambers' geometry was approximated with simple geometric shapes. The atria were both considered as spheres, the left ventricle as a half ellipsoid and the right ventricle as a quarter of an ellipsoid (Figure 1). Throughout the text, all parameters and variables that change with time are indicated with lower-case letters, whereas constant parameters are indicated with upper-case letters. All chambers were characterized by an inner radius r and a wall thickness h . The length of the ventricular ellipsoidal shapes was set to $3r$, based on clinical data (45). No interatrial nor interventricular septal interactions were taken into account. Based on these assumptions, wall and chamber volumes were calculated as follows. Equations (1) and (2) represent the atrial cavity volume and the atrial myocardial wall volume, respectively. Similarly, equation (3) and (4) represent the left ventricular (LV) cavity volume and the LV myocardial wall volume. The volume of the right ventricular (RV) cavity and RV wall volume are calculated as half of equation (3) and (4).

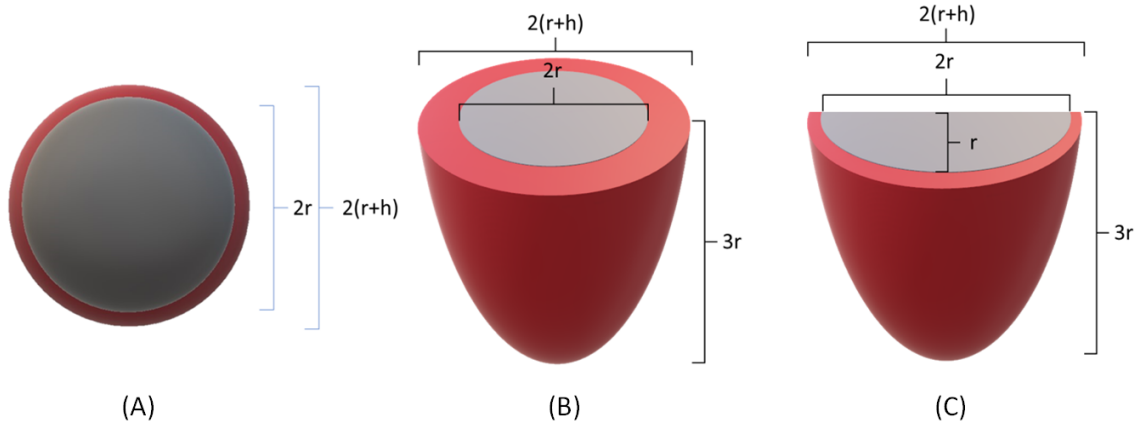


Figure 1. (A) Atria. Both the left and right atrium are approximated to be spheres with an inner radius of r , a wall thickness of h , an inner blood volume of v and a wall volume of v_{wall} . (B) Left ventricle. The left ventricle is approximated to be a half ellipsoid with max inner radius r , wall thickness h and a length of $3r$. (C) Right ventricle. The right ventricle is approximated to be a quarter ellipsoid with max inner radius r , wall thickness h and a length of $3r$.

$$v = \frac{4 \cdot \pi \cdot r^3}{3} \quad (1)$$

$$v_{wall} = \frac{4 \cdot \pi \cdot (r + h)^3}{3} - \frac{4 \cdot \pi \cdot r^3}{3} \quad (2)$$

$$v = \frac{1}{2} \cdot \frac{4 \cdot \pi \cdot 3r \cdot r^2}{3} = 2 \cdot \pi \cdot r^3 \quad (3)$$

$$v_{wall} = \frac{1}{2} \cdot \frac{4 \cdot \pi \cdot (3r + h) \cdot (r + h)^2}{3} - 2 \cdot \pi \cdot r^3 \quad (4)$$

Myofiber stress and wall shear stress definition

Instantaneous σ_f was calculated as indicated in equation 5, based on previous work by Arts et al (1). Myocardial σ_{wss} was calculated assuming a laminar flow through a tube with the same diameter as the largest chamber diameter (equation 6), analogous to vascular tissue remodeling (35). Chamber flow $q_{chamber}$ was calculated as the mean value of absolute inlet and outlet flows at each time step in the simulation, as shown in equation 7. In such a way, σ_{wss} is affected by both antegrade and retrograde flow. If no regurgitant valve flows or shunts are present, then mean $q_{chamber}$ equals cardiac output. In regurgitant valve disease, $q_{chamber}$ becomes considerably larger than cardiac output because the absolute value of both forward and backward flows are taken into account.

$$\sigma_f = p \cdot \frac{3}{\ln \left(1 + \frac{v_{wall}}{v_{lumen}} \right)} \quad (5)$$

$$\sigma_{wss} = \frac{4 \cdot \eta \cdot q_{chamber}}{\pi \cdot r^3} \quad (6)$$

$$q_{chamber} = \frac{|q_{inlet}| + |q_{outlet}|}{2} \quad (7)$$

Variables and constants. σ_f = chamber myofiber stress, p = chamber intracavitary pressure, \ln = natural logarithm operator, v_{wall} = chamber wall volume, v_{lumen} = chamber intracavitary blood volume, σ_{wss} = chamber wall shear stress, η = blood viscosity, $q_{chamber}$ = chamber blood flow, r = chamber radius, q_{inlet} = inlet valve blood flow, q_{outlet} = outlet valve blood flow.

Myocardial volume adaptation

The first remodeling rule determines the adaption of myocardial wall volume by preservation of σ_f . Total myocardial volume was assumed to be 160 mL based on a generic adult person of 70 kg and 170 cm length with a body surface area of 1.81 m². We assumed that the myocardium was distributed among the four cardiac chambers in proportion to the sum of the passive stiffness constant and the systolic contractility (see Appendix for further details). Then,

remodeling rules were activated, and parameters reached the values presented in Table 1. This set of parameters was the starting point of the valve disease simulations.

Table 1. Start values representing normal physiology at mean wall shear stress 0.0025 mmHg and mean myofiber stress 120 mmHg in all chambers. Gray columns show baseline elastance values and white columns chamber dimensions derived from elastance values using the geometric assumptions and remodeling algorithms described in the main text.

	Passive stiffness constant	Systolic contractility	Sum	Wall volume	Chamber diameter	Wall thickness
	<i>mmHg/mL</i>	<i>mmHg/mL</i>	<i>mmHg/mL</i>	<i>mL</i>	<i>mm</i>	<i>mm</i>
RA	0.097	0.065	0.162	6	48*	0.9*
RV	0.012	0.599	0.611	24	68/50**	2.7/4.5**
LA	0.144	0.103	0.247	10	47*	1.3*
LV	0.021	2.735	2.753	108	54/39**	8.2/12.8**
TOTAL	0.274	3.502	3.776	148		

RA = right atrium, RV = right ventricle, LA = left atrium, LV= Left ventricle.

* mean value, ** end-diastolic/end-systolic.

The target σ_f was set to 120 mmHg in each cardiac chamber. This value was chosen as it provided physiological arterial pressure and cardiac output. The wall volume was assumed proportional to the total elastance and adjusted until the target σ_f was reached. The total myocardial volume was updated accordingly. Both stiffness constant and contractility were changed proportionally (see appendix for definitions and further details). This means that an increase in contractility was assumed to be accompanied by an increase in passive stiffness as is seen in many patients with clinical LV hypertrophy due to structural valve disease or hypertension (30, 42, 51).

Chamber volume adaptation

The second remodeling rule determines the adaption of chamber volume in order to preserve σ_{wss} , with a target value of 0.0025 mmHg (see Appendix for target value selection criteria and sensitivity). The adaptation operates as follows: σ_{wss} is continuously calculated during simulations as in equation 2. Then, the volume intercept V_0 of the elastance function of each

chamber is adjusted until a target σ_{wss} value of 0.0025 mmHg is reached. A change in V_0 can be interpreted as a change in the unstressed chamber volume by adding/removing or elongating/shortening sarcomeres in series within the cardiomyocyte.

The two rules act simultaneously and myocardial σ_f and σ_{wss} interact mutually because (i) they are both affected by changes in chamber size and (ii) the wall volume and the chamber volume are both determinants of stress. In general, dilatation of a chamber will lead to an increase in σ_f , which in turn requires an increase in wall volume and wall thickness to preserve σ_f .

Simulation of valvular disease

Aortic stenosis was simulated by incrementally decreasing the open aortic valve area from 5.0 cm² to 0.5 cm² in steps of 1.00 cm² for the mild range and steps of 0.25 cm² for the severe range. Mitral regurgitation was simulated by increasing the closed mitral valve area from 0.0 cm² to 0.80 cm² in steps of 0.10 cm², corresponding to regurgitant fractions from 0% to 54%. Aortic regurgitation was simulated by increasing the closed aortic valve area from 0.0 cm² to 0.45 cm² in steps of 0.05 cm², corresponding to a regurgitant fraction increase from 0% to 61%. Heart rate, vascular properties and blood volume were kept unchanged. Consequently, no autoregulatory or compensatory mechanisms were included in the simulations, other than cardiac remodeling. The pericardium was allowed to remodel in size (41) to create a mean pericardial pressure of 0 mmHg – therefore the pericardium did not constrain the heart. Notably, vascular properties were kept unchanged in the simulation study. In this way, possible confounding factors were limited, increasing the correlation between the regurgitant/stenotic valve area and degree of remodeling.

Additionally, the independent effect of σ_{wss} and σ_f adaptation was tested by simulating various degrees of aortic regurgitation while preserving only one variable at the time. First, σ_{wss} adaptation was allowed, but not σ_f , and then vice versa.

Calculations

Simulations were run using the software Aplysia CardioVascular Lab 7.0.4.11 (Aplysia Medical AB, Stockholm, Sweden). Mean values in the model were calculated as a weighted running average with recent values having more impact than older ones (see appendix for details). Intrathoracic pressure changes due to respiration were omitted in the simulations. Hemodynamic differential equations were solved with implicit or explicit Euler's method, while wall thickness 3rd degree polynomial equations were solved with Newton-Raphson's

method. Pressures, flows, volumes and saturations in every compartment were calculated with a frequency of 4000 Hz. Calculations and adaptation of σ_f and σ_{wss} algorithms were implemented in the software and run automatically, reaching stable steady-state values within 5 minutes. This implies that acute hemodynamics were simulated in real-time, but remodeling was simulated in a time-scale at least 10,000 times faster than in real physiology (50,000 minutes corresponding to 35 days). All data were collected at end-diastole when simulations had reached a steady-state regarding remodeling, hemodynamics and oxygen transport.

Comparison with clinical data

Simulation results were compared with published clinical data on LV mass and volume for aortic stenosis (14) and mitral and aortic regurgitation (47). Specifically, the data were extracted from Uretsky et al. (47) by calculating the desired variable y using the regression equation reported in the reference, with x equal to the simulated regurgitant flow. Simulation outputs were then compared with patients' values in a quantitative manner by looking at the slope and offset of the linear regression lines. When such data were not available in the reference studies (14, 47), a qualitative comparison of remodeling patterns in simulations and patients was performed. The different LV remodeling patterns were classified as follows (i) concentric remodeling: LV diameter preserved or reduced with wall volume increase below clinical detection limit of current imaging techniques; (ii) concentric hypertrophy: LV diameter preserved or reduced with increase in wall volume; (iii) eccentric remodeling: LV diameter increased in size with wall volume increase below clinical detection limit; (iv) eccentric hypertrophy: LV diameter increased with increase in wall volume.

Results

Simulation output for the three different valvular diseases are shown in Figure 2 and are described in the following sections including a quantitative comparison with published clinical data. Figure 2 shows a summary of the simulation for the three valvular diseases investigated. The regurgitant/stenotic valve area is reported as a label at each simulated step. Aortic stenosis showed a concentric remodeling pattern (decrease in LV end-diastolic volume) accompanied by large increase in LV wall volume, especially for the most severe cases. On the contrary, aortic and mitral regurgitation show an eccentric remodeling pattern with increased LV end-diastolic volume. Aortic regurgitation showed a more pronounced hypertrophy (increase in LV wall volume) than mitral regurgitation. Additional hemodynamic outputs are presented in Table 2.

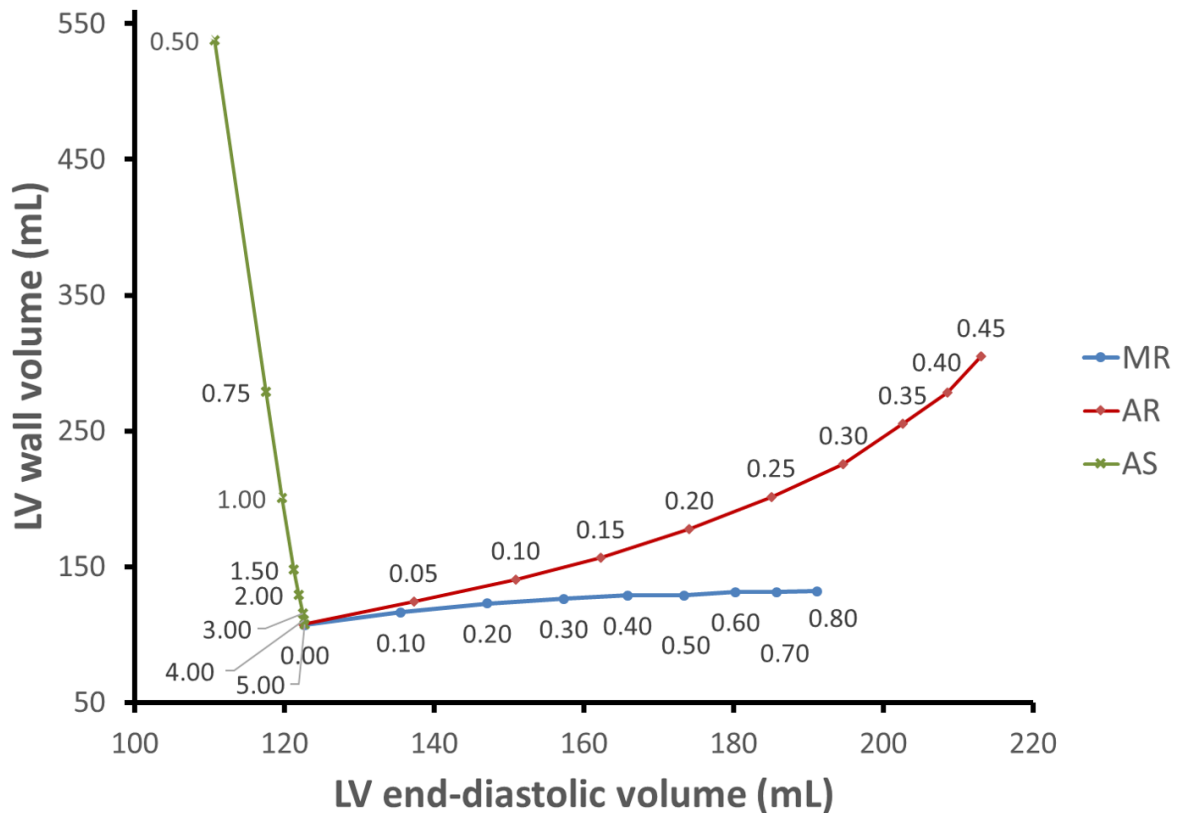


Figure 2. Simulation output of changes in left ventricular end-diastolic volumes and wall volumes in valvular disease with varying valve areas. Aortic stenosis (AS), mitral regurgitation (MR) and aortic regurgitation (AR). Valve areas for each simulation step are indicated in the figure. AS result in concentric hypertrophy and AR and MR in eccentric hypertrophy (more pronounced hypertrophy in AR).

204

205 Aortic stenosis

206 Simulations of aortic stenosis with adaptive remodeling showed that systolic arterial pressure
 207 and cardiac output at rest were preserved until the aortic valve area reached approximately
 208 1.5 cm^2 . For smaller areas, systolic pressure dropped from 118 mmHg to 105 mmHg in the
 209 most severe case, with a maximum aortic valve area of 0.5 cm^2 , and cardiac output changing
 210 from 5.7 L/min to 5.1 L/min. Diastolic arterial pressure was essentially preserved. Resulting
 211 LV geometries are shown in Figure 3. The LV hypertrophied for aortic areas below 1.5 cm^2 .
 212 LV diastolic wall thickness increased from 10.7 mm to 28.0 mm when the aortic valve area
 213 decreased between 1.5 cm^2 and 0.5 cm^2 . At the same time, the LV preserved its diameter until
 214 valve areas fell below 1.0 cm^2 and slightly decreased in the most severe case. The LA preserved
 215 its size. The results suggest that a normal LV internal diameter is preserved down to an aortic

valve area of approximately 2 cm². For more severe stenosis, the LV showed a concentric remodeling pattern down to a valve area of 1.5 cm². For the most severe stenosis areas, the LV geometry can be classified as concentric hypertrophy. Simulation output are in agreement with data from patients with aortic stenosis (18), although patients in the study by Dweck *et al.* (14) exhibited different LV remodeling patterns: normal LV, concentric remodeling and concentric hypertrophy, both symmetric and asymmetric.

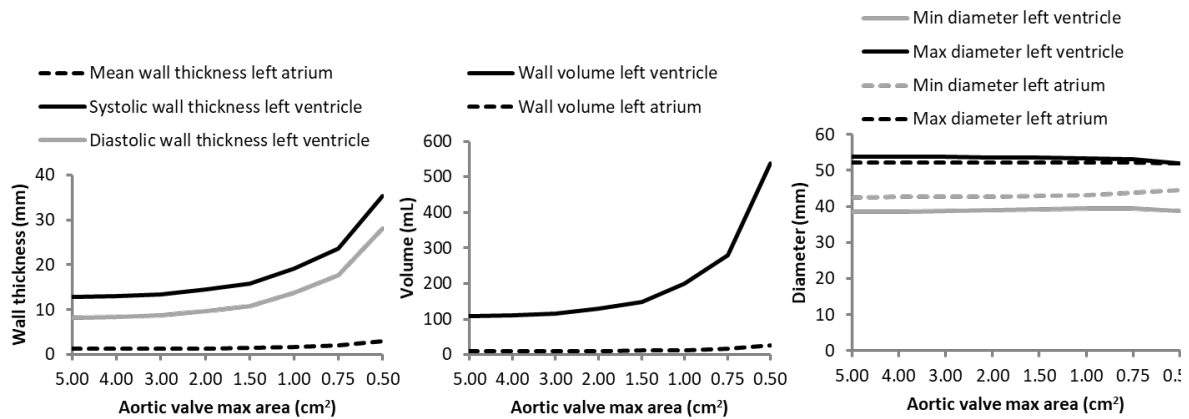


Figure 3. Simulation output of different degrees of severity of aortic stenosis with myocardial remodeling. A small aortic opening area results in a large increase in systolic and diastolic wall thickness, left ventricular wall volume and a slight decrease in chamber diameter.

Mitral regurgitation

Simulations of mitral regurgitation with adaptive remodeling showed that systemic arterial blood pressure decreased from 122/76 (systolic/diastolic) mmHg with no regurgitant volume to 100/63 mmHg in the most severe case, with a minimum mitral valve area 0.8 cm^2 , regurgitant volume of 67 mL corresponding to a regurgitant fraction of 54%. Cardiac output decreased from 5.7 L/min to 4.1 L/min. Resulting LV geometries are shown in Figure 4. LV diastolic wall thickness decreased from 8.2 mm to 7.8 mm, whereas total LV wall volume increased from 107 mL to 132 mL. The LV enlarged by increasing its diastolic diameter from 54 mm to 62 mm. The LA also increased its diameter to a similar degree. The results represent a LV eccentric remodeling pattern.

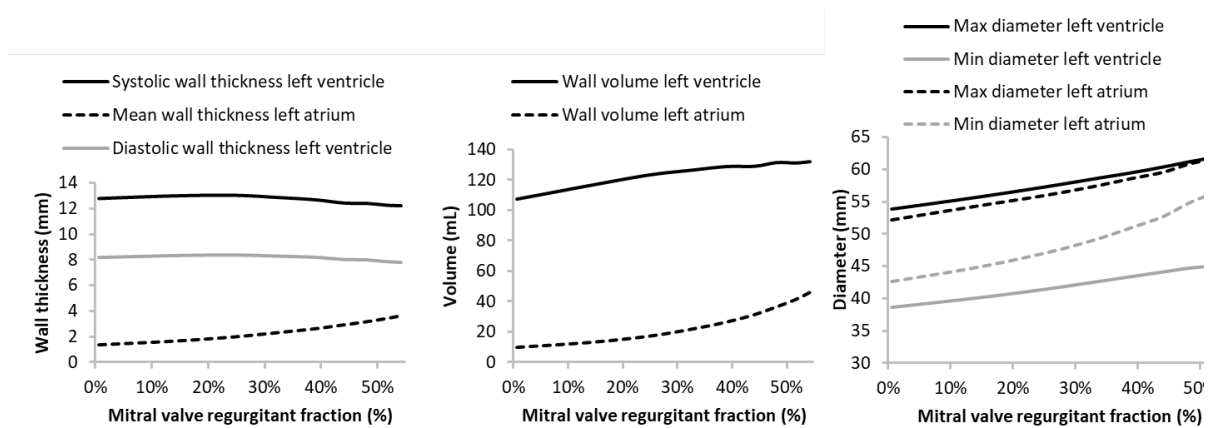


Figure 4. Simulation output of different degrees of severity of mitral regurgitation with myocardial remodeling.

When comparing simulation results with clinical data (Figure 5), it can be seen that they follow the same direction of changes for LV end-diastolic volume index (EDVI), end-systolic volume index (ESVI), LV end-systolic diameter (ESD) and LA volume. Also, slopes and offset agreed well in magnitude with clinical data, as shown by the linear regression equations in Figure 5.

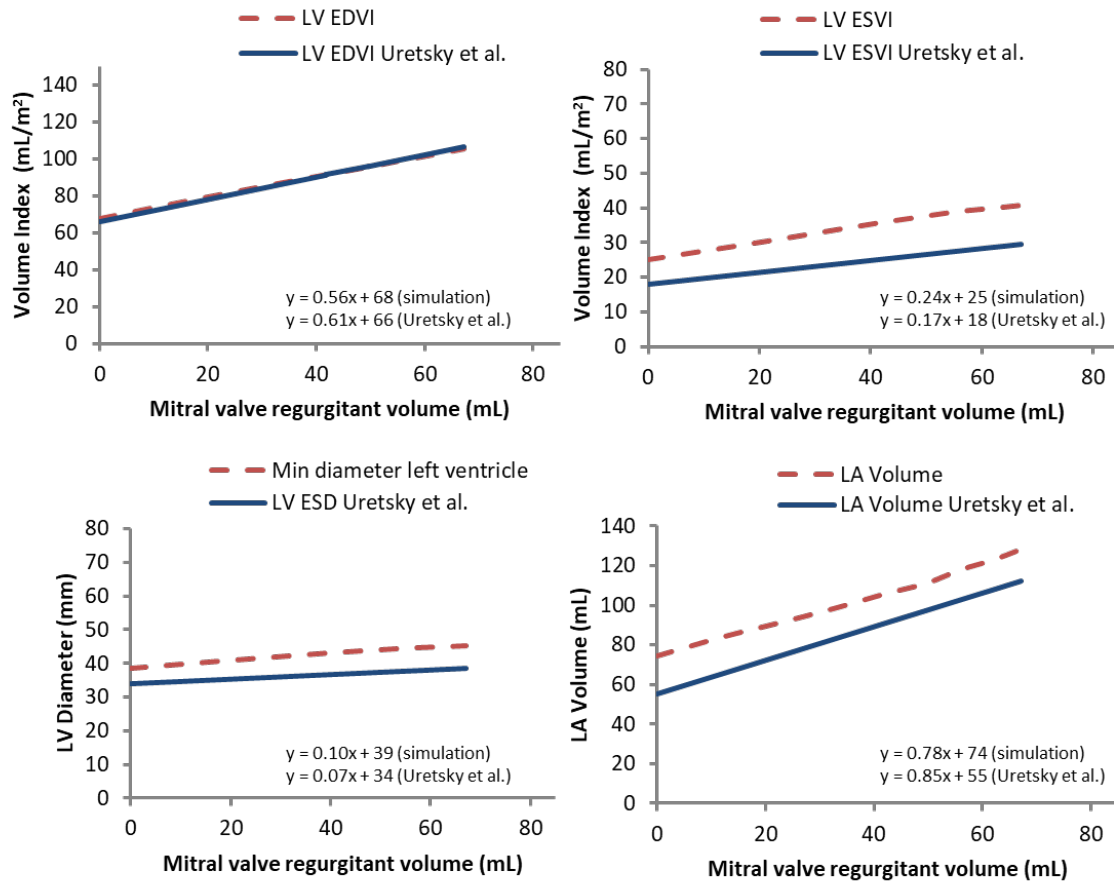


Figure 5. Comparison between simulation output in mitral regurgitation and clinical data from Uretsky et al. (47). The linear regression equations are shown in the lower part of each panel.

Aortic regurgitation

Simulations of aortic regurgitation with adaptive remodeling showed that systolic arterial pressure was preserved from the normal initial case to the most severe case, with a regurgitant aortic valve area of 0.45 cm², regurgitant volume of 83 mL, and regurgitant fraction of 61%. Diastolic arterial pressure decreased from 76 mmHg to 44 mmHg between the same two scenarios. Cardiac output decreased from 5.7 L/min to 4.0 L/min. Resulting LV geometries are shown in the upper row of Figure 6. LV diastolic wall thickness increased from 8.2 mm to 14.7 mm. The LV hypertrophied and enlarged by increasing its wall volume from 108 mL to 305 mL and its diastolic diameter from 54 mm to 65 mm. The LA did not enlarge but became slightly smaller in the most severe cases. The results represent a LV eccentric remodeling pattern with hypertrophy.

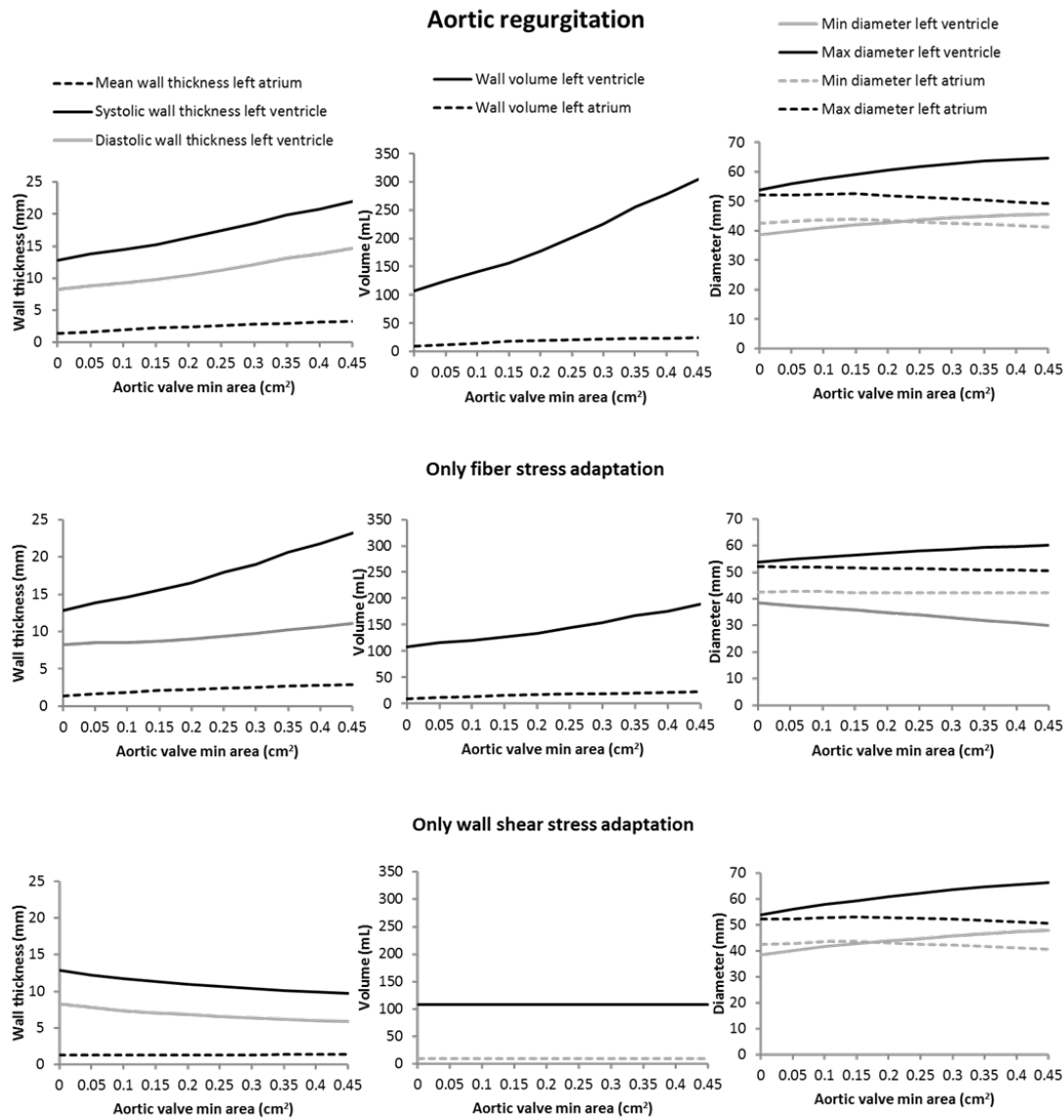


Figure 6. Simulation output of different degrees of severity of aortic regurgitation with complete myocardial remodeling based on both fiber stress and wall shear stress in the upper row. The middle row shows adaptation of fiber stress excluding adaptation of wall shear stress and the bottom row adaptation of wall shear stress excluding adaptation of fiber stress. Wall shear stress induced dilatation and wall thinning occurs in the bottom row, while wall volume increase with wall thickening occurs in the middle row with only fiber stress adaptation. Both mechanisms are needed for a realistic adaptive remodeling process as seen in the upper row.

251

252

253

254

When comparing simulation results with clinical data (Figure 7) for LV EDVI, ESVI, LV ESD and LV end-diastolic diameter (EDD), all four variables agreed in terms of direction of changes. Also, LV diastolic and systolic diameters agreed very well in magnitude compared to clinical

data, whereas LV EDVI and LV ESVI increased less in simulations than in the clinical data as can be seen in the lower slopes of the simulation regression lines in Figure 7.

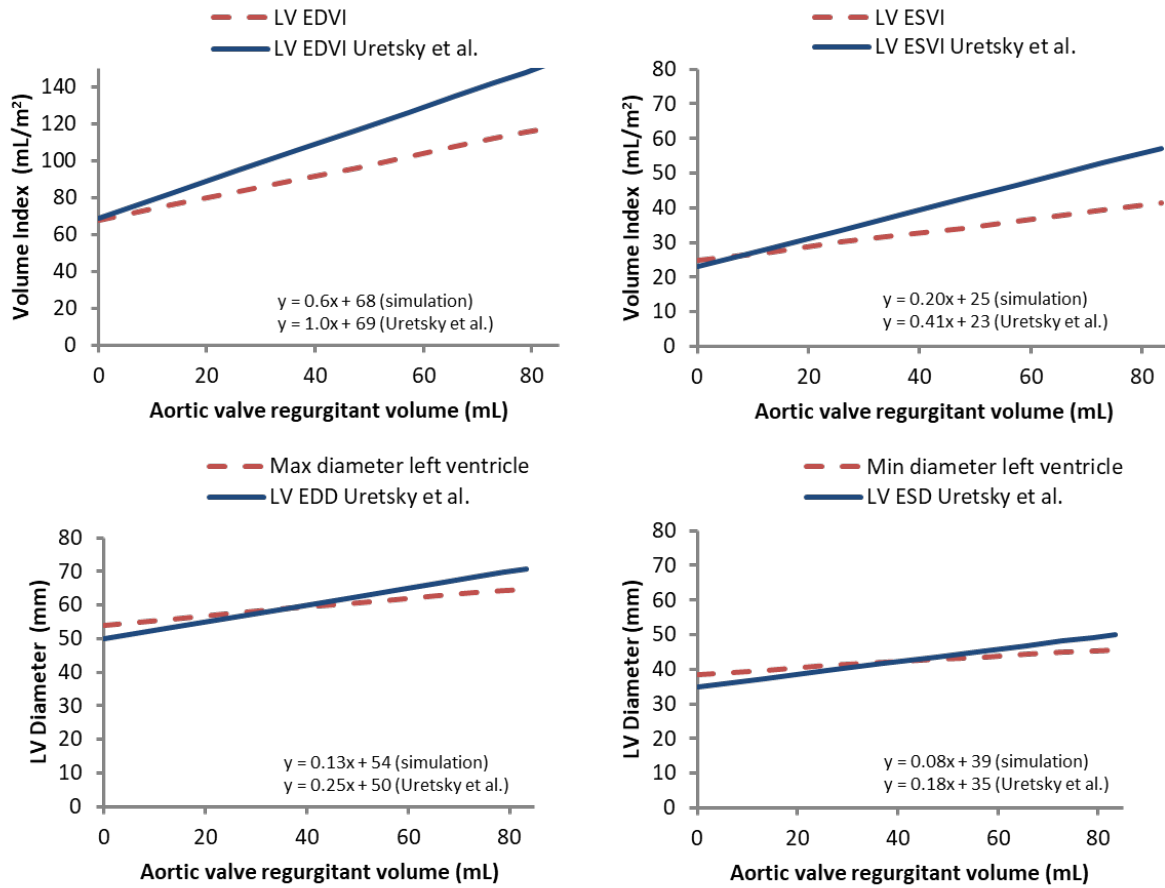


Figure 7. Comparison between simulation output in aortic regurgitation and clinical data from Uretsky et al. (47). The linear regression equations are shown in the lower part of each panel.

Isolated effect of wall shear and fiber stress adaptation in aortic regurgitation

The middle and lower rows of Figure 6 show the output of the simulations when the two adaptation rules were activated separately. σ_f adaptation alone resulted in an increasing wall volume. The small changes seen in LV size is caused by the regurgitation contributing to filling combined with the increased contractility and stiffness associated with increased wall volume. On the contrary, σ_{wss} adaptation alone caused the LV to remodel in an eccentric manner (both minimum and maximum diameter increased with increasing regurgitant volume), whereas wall volume remained constant. Notably, despite wall volume not changing, wall thickness decreased as a consequence of LV enlargement. The combined effect of the two adaptation

rules in aortic regurgitation are shown in the upper row of Figure 6 and illustrates the interaction, where σ_{wss} induced dilatation results in higher σ_f and therefore a need for a more pronounced wall volume increase to preserve fiber stress.

Table 2. – Main hemodynamic variables (simulation output) for the normal case and three different degrees of severity of valve diseases.

Area	Systolic arterial pressure	Diastolic arterial pressure	Mean arterial pressure	Cardiac output	LV Ejection fraction	RV Ejection fraction	LA pressure	RA pressure
<i>cm²</i>	<i>mmHg</i>	<i>mmHg</i>	<i>mmHg</i>	<i>L/min</i>	-	-	<i>mmHg</i>	<i>mmHg</i>
Baseline								
0/5.00	122	76	95	5.73	0.65	0.65	6.9	4.3
Mitral regurgitation								
0.3	113	70	86	4.99	0.65	0.65	9.9	4.0
0.6	104	65	78	4.39	0.65	0.65	12.4	3.7
0.8	100	63	74	4.11	0.65	0.65	13.7	3.6
Aortic regurgitation								
0.2	123	60	83	4.82	0.64	0.65	10.7	4.1
0.3	129	50	77	4.37	0.65	0.65	13.3	3.9
0.5	131	44	71	3.95	0.65	0.65	16.0	3.9
Aortic stenosis								
3.00	121.45	76.52	94.67	5.72	0.65	0.65	6.8	4.3
1.00	115.51	76.11	93.22	5.59	0.65	0.65	8.4	4.2
0.50	105.24	72.49	87.24	5.11	0.65	0.65	13.8	3.9

Discussion

The major finding of this study is that our cardiovascular simulation of cardiac remodeling in valvular disease based purely on mechanical factors accurately predicts typical remodeling patterns seen in patients. The heart changes its size in conjunction with its myocardial volume in order to preserve a target σ_{wss} and σ_f and the resulting geometry is validated against high-resolution MRI imaging (14, 47) (Figures 2, 4 and 6). Simulations show that σ_f is the main determinant of hypertrophy (wall volume changes) and σ_{wss} the main determinant of LV size confirming our initial hypothesis. Wall volumes, chamber diameters, wall thickness and end-diastolic compliances are all within an expected range (6, 15, 19).

Cardiac remodeling is a complex, multifactorial process, which is importantly driven by changes in myocardial loading conditions as a result of e.g. stenotic or regurgitant valves. Results from this study support the hypothesis that preservation of the clinically accessible biomechanical factors σ_f and σ_{wss} can explain cardiac remodeling patterns in valvular heart disease. It should however be mentioned that genetic factors and comorbidities such as hypertension also play a role and may result in interindividual variation despite similar valve pathology (37). Our findings are in agreement with a previous simulation study showing that a model based on passive and active properties of the individual sarcomeres and with mechano-adaptive control could determine chamber size and myocardial wall volume of all four cardiac chambers in normal physiology (3), but in contrast to this study we use input data extractable from clinical diagnostic imaging and test the algorithms in a different range of loading conditions by including valve pathology.

Such simulations models have e.g. been used to explain cardiac chambers size based on fiber stress (σ_f) optimization (3), to reproduce wave dynamics throughout the circulation (32), to explain blood pressure changes with aging (27), to monitor cardiac loading conditions during mechanical support (7, 13), and could be valuable to differentiate and quantify mechanical overload-induced cardiac remodeling in individual patients.

While simulation results from this study show how mechanical triggers may be important factors in cardiac remodeling, they cannot uniquely identify which mechanical variables are the actual drivers of remodeling. σ_f and σ_{wss} are good candidates given the agreement between simulations and clinical data. However, other variables such as fiber strain (2) could be complementary driving factors contributing to remodeling. It is intriguing that when calculating myofiber shortening (strain) according to Arts *et al.* (1) (Figure 8) in remodeled AS, it decreases with stenosis severity in agreement with clinical findings (44) despite preserved ejection

fraction and increasing LV contractility (end-systolic elastance). The decrease in fiber shortening (strain) in clinical measurements has been interpreted as a sign of decline in systolic function (33) but should probably rather be seen as a geometric consequence of wall thickening in combination with high afterload (44). These clinical and simulation findings speak against preservation of strain as the principal biomechanical factor determining chamber size, but deserve further in-depth analysis, to elucidate the precise relation between modeled myofiber strain on one hand and longitudinal and epi-/endo-cardial circumferential strain as measured clinically on the other.

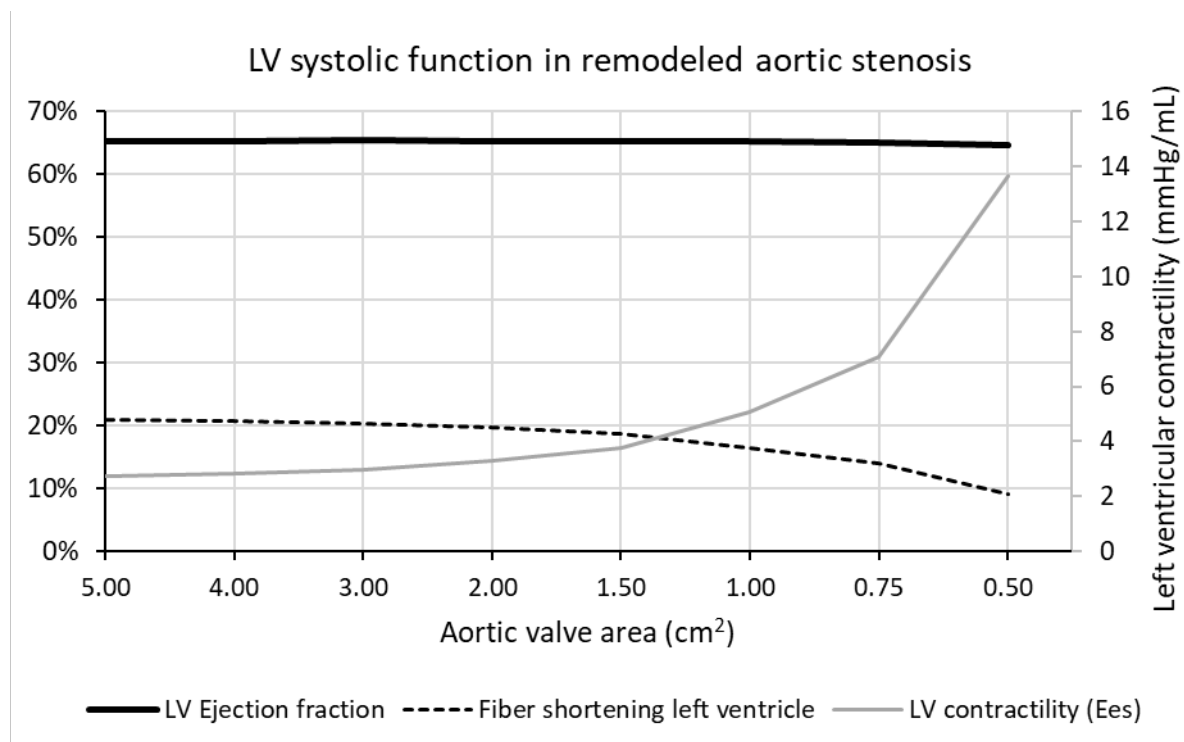


Figure 8. Measures of systolic function in simulated remodeled aortic stenosis. Ejection fraction (black) is preserved, while elastance (gray) increases with valve stenosis severity. Myofiber shortening (strain) (dashed black) decreases with valve narrowing and increasing hypertrophy.

Simulations of the disease process can be seen as a longitudinal study on a single individual as disease severity progresses. However, clinical data conventionally available like those used for validation in this study (14, 47) are single time point measurements providing a cross-section of multiple individuals with different degrees of disease severity.

Simulations of aortic stenosis produced a concentric remodeling pattern with pronounced LV hypertrophy for the most severe cases (Figure 3). Patient data reported by Dweck et al. (14) showed many different kinds of LV remodeling patterns in response to aortic stenosis, including normal LV and LV decompensation. LV decompensation occurs in the late stages of the

diseases when the myocardium cannot adapt to load changes anymore and therefore the remodeling rules cannot be met. This structural limit of the myocardium, possibly influenced both by mechanical material properties and ischemia, has not been included in the modeling assumption and therefore LV decompensation cannot be predicted with the current model implementation. The simulation could however predict the other compensatory LV geometries observed in patients. Firstly, simulations show that aortic maximal area must be small ($< 1.5 \text{ cm}^2$) before the LV begins to remodel. This implies that the LV can preserve a normal geometry down to this aortic valve area. When the adaptive remodeling process starts, it manifests initially as concentric remodeling and ultimately as concentric hypertrophy (Figure 2). Dweck et al. reported no correlation between aortic area measurements and degree of LV hypertrophy, which probably is due to a quite narrow range of valve areas ($0.93 \pm 0.32 \text{ cm}^2$). Other authors with larger span of aortic valve areas have found a clear relationship with hypertrophy and found that wall thickness increased proportional to the increase in left ventricular systolic pressure, preserving wall stress (18). In addition, other individual factors that influence hypertrophy such as genetic background and additional comorbidities e.g. hypertension, diabetes and obesity will influence hypertrophy, and this is not taken into account in the simulations. Finally, non-invasive measurements of effective valve area are prone to measurement errors, also with MRI. The clear correlation between aortic area and LV mass in the simulations, occurs mainly for very small aortic areas ($< 0.75 \text{ cm}^2$). Some of the discordance between clinical results and simulations can be explained by the difficulty of measuring these small areas of the stenotic aortic valve using *in vivo* imaging methods, which have limited spatial resolution (echocardiography and MRI both $> 1\text{-}2 \text{ mm}$ (16)). In addition, the generally irregular shape of the stenotic aortic valve area might be of hemodynamic importance. Taken together, the net aortic valve area derived from medical imaging may not be the most robust measurement of disease severity.

Simulations showed that mitral and aortic regurgitation resulted in an eccentric remodeling pattern (Figures 4 and 6) in accordance with patient data (47) (Figures 5 and 7). Aortic regurgitation produced a clear hypertrophy of the LV, whereas mitral regurgitation resulted in only a mild hypertrophy (Figure 2), due to a progressive decrease in afterload with worsening regurgitation, since part of the LV output is ejected retrogradely into the low-pressure atrium instead of into aorta. Simulations also showed that the LA increased its size in mitral regurgitation but not in aortic regurgitation, where the opposite was seen, that is a slight decrease in LA size for the most severe cases (Figures 4 and 6). The decrease in LA size in aortic regurgitation may be explained by a decrease in cardiac output, due to lack of

autoregulatory control mechanisms preserving systemic flow in our study. The clinical data reported by Uretsky et al. (47) showed poorer correlation between mitral regurgitant volume and LV ESVI ($r^2 = 0.5$) and LA volume ($r^2 = 0.3$) than with LV EDVI ($r^2 = 0.8$). The lack of compensatory baroreflex mediated sympathetic activity in the simulations may explain the slightly larger simulated end-systolic volumes in mitral regurgitation (Figure 5). Our simulations showed however that all three variables are clearly correlated to mitral regurgitant volumes (Figure 5). LV EDVI is the largest of these volumes and it increases the most with increased regurgitant volume, which makes it an easier and more robust variable to measure. In the simulation results for mitral regurgitation, it can also be noticed that mild hypertrophy (defined as an increase in wall volume) does not manifest as an increase in wall thickness, which slightly decreases due to the LV dilatation. Previous simulation work in aortic regurgitation has shown how parameters such as ventricular and aortic wall properties can influence hemodynamic output in a way that is not captured by clinical severity scores (34). Simulations can highlight the most important factors to take into account and clinically measure when evaluating a given disease state in general or more specifically the expected remodeling pattern in an individual patient. As an example, simulations indicate that wall volume or mass-cavity ratio might be alternative indexes of disease severity worthy of clinical evaluation.

Limitations

Actual σ_{wss} and σ_f values are currently difficult to measure *in vivo* (see appendix for current σ_{wss} and σ_f selection criteria). A recent study (29) reports MRI estimated mean σ_{wss} in the human left ventricle in the range 0.2-0.6 Pa corresponding to 0.0015-0.0045 mmHg supporting the target value 0.0025 mmHg used in the current study. The target value for mean myofiber stress 120 mmHg is supported by Genet *et al* (17) estimating a normal human operating LV myofiber stress range of 2.2-16.5 kPa (16.5-124 mmHg) and Lee et al (25) estimating peak LV myofiber stress to 50-80 kPa (375-600 mmHg) in a group of patients post cardiac surgery due to heart failure. In the absence of more detailed information, we have applied the same values for all four chambers. Refined geometrical assumptions and data from future 3D simulation studies may provide more precise input data that may result in e.g. more realistic atrial sizes. More specifically, our geometrical assumptions about the RV may need refinement in future studies concerning right-sided lesions or pulmonary hypertension, since the infundibulum and RV outlet tract is not taken into consideration in our simplified geometry. The equations relating wall volumes to chamber volumes assume a geometry with rotational symmetry, which is true for the atria and left ventricle, but not for the right ventricle. This would also be a significant

limitation, when applying the model to right-sided lesions or pulmonary hypertension, but does not affect our conclusions, since right-sided changes are negligible in this study.

The calculation of σ_{wss} was based on the assumption of laminar flow through a tube, which is an oversimplification of reality. In fact, the LV shows vortical flow patterns (4). In general, vortexes can be both laminar and/or turbulent and which pattern is seen in ventricular flow is still under investigation (10, 22). This implies that the calculated σ_{wss} might not correspond to the actual σ_{wss} experienced by the chamber walls. However, the target σ_{wss} value was chosen in order to provide physiological hemodynamic output for a normal individual. This simplified assumption will only affect the magnitude of the simulation output during remodeling, but not the overall direction of changes.

The present model cannot represent 3D features of the circulatory system. Also, we have assumed homogenous wall thickness. It is likely that differences in σ_f and impact of σ_{wss} exist within the myocardial walls. Dweck et al. (14) report both symmetric and asymmetric remodeling, patterns that cannot be predicted by the type of modeling used in this study (lumped-parameter 0D modeling), which does not provide local 3D information and therefore asymmetric remodeling falls into the concentric remodeling and hypertrophy patterns. However, 0D modeling allows real-time simulation with a standard PC and is therefore a more realistic clinical decision support tool.

Compensatory mechanisms such as baroreceptor effects and changes in blood volume to preserve cardiac output were not included in the simulations and neither was vascular remodeling. These mechanisms may explain some of the differences between simulation results and clinical data. Future clinical application of the model may have to include the autoregulatory features of the cardiovascular system.

A crucial clinical question is how to differentiate between adaptive and maladaptive remodeling. Unfortunately, this question is currently unresolved and also not well understood in clinical medicine. We can only speculate about ischemia, progressive fibrosis with negative diastolic and systolic effects and exhaustion of the Starling mechanism driven by changes in collagen subtypes, oxidative stress, inflammation, neurohormonal activation and mitochondrial dysfunction (39). Providing “rules” for adaptive remodeling could potentially make it easier to draw the line between adaptive and maladaptive responses through the course of myocardial load history. It is likely not possible to fully understand the maladaptive response without a more detailed simulation of the myocardial sub-cellular structure including vascular supply.

Sex and ethnic differences have not been taken into account, which is mainly due to lack of suitable validation studies, but also due to lack of biomechanical hypothesis explaining such differences. Future studies taking not only these factors, but also body size and comorbidities are needed to explore these questions. Importantly, this model-based approach allows to simulate and predict on an individual basis rather than on a group level, which creates an important future advancement towards patient-specific, individualized cardiovascular diagnostics and therapeutics.

Clinical implications

The importance of remodeling in clinical cardiac disease is indisputable. By being able to calculate, predict and differentiate the adaptive part of remodeling from other pathological processes such as ischemia, tissue fatigue and genetic disorders, it may be possible to better predict what reversibility can be expected after interventions and better differentiate primary from secondary changes in structural heart disease. Patient-specific simulation of remodeling may therefore in the future aid in decision-making related to interventions and drug therapy.

Conclusions

Computer simulations of remodeling show that biomechanical factors alone can explain the major remodeling patterns (eccentric vs concentric LV hypertrophy) seen in left-sided valvular heart disease. These findings both qualitatively and quantitatively support the hypothesis that chamber size and degree of hypertrophy to a large extent can be explained by preservation of myocardial fiber stress and wall shear stress. Additional clinical and experimental studies in different pathologies are needed to further validate these results and potentially refine the modeling assumptions.

Appendix

Additional information about the model and simulation methods are presented in the following sections.

Cardiovascular model overview

The cardiovascular model used in this study is constituted of multiple lumped-parameter segments of the circulatory system and has previously been described (8). The four cardiac chambers are modeled as time-varying elastances, the arterial segments are modeled as 4-element Windkessel models and the cardiac valves change their area gradually during opening and closing (31). The function of the pericardium to prevent cardiac enlargement and the motion of the intraventricular septum are also included in the model. The reader is referred to the article by Broomé et al. (8) for a full description of the model structure and strategies for parameter selection. Some selected definitions and model equations useful for this specific study are described below.

Definitions

Variables changing with time are indicated with lower-case letters. Constant parameters are indicated with upper-case letters.

The time-varying elastance $e(t)$ in each cardiac chamber is defined by the Double-Hill equation (eq. 1.A):

$$e(t) = e_{max}(v_{ed}, q) \cdot a \cdot \left[\frac{\left(\frac{t}{\alpha_1 \cdot T}\right)^{n_1}}{1 + \left(\frac{t}{\alpha_1 \cdot T}\right)^{n_1}} \cdot \frac{1}{1 + \left(\frac{t}{\alpha_2 \cdot T}\right)^{n_2}} \right] + e_{min}(v) \quad 1.A$$

v_{ed} is the end diastolic volume, q is the flow through the outflow valve of the chamber, t is the time, T is the time period of one heart cycle, α_1 , α_2 , n_1 and n_2 are dimensionless constants determining the shape of the elastance curve and thereby the duration of contraction and relaxation. $e_{min}(v)$ is a variable elastance defining the diastolic pressure-volume relation as further described in equation 3A.

The value of e_{max} varies in a way that reproduces the Frank-Starling mechanism according to eq. 2.A:

$$e_{max}(v_{ed}, q) = E_{max} \cdot \left[1 - \left(\frac{v_{ed}}{V_{ed,max}} \right)^4 \right] \cdot \left[1 - \frac{q}{Q_{max}} \right] \quad 2.A$$

480

481 Where E_{\max} is the systolic contractility constant, $V_{\text{ed},\max}$ is the maximum chamber volume
482 defining the curvature of the end-systolic elastance and Q_{\max} the maximum flow in the
483 corresponding chamber representing the internal chamber flow resistance (8).

$$e_{\min}(v) = E_{\min} \cdot e^{\sigma \cdot (v-v_0)} \quad 3.A$$

484 Where E_{\min} is the passive stiffness constant, σ is a constant factor regulating the shape of the
485 diastolic elastance curve and v_0 is the volume at which the end-systolic pressure volume
486 relationship meet the volume axis in a pressure-volume diagram, representing the unstressed
487 chamber volume.

488 E_{\max} and E_{\min} are constant values and are referred to as systolic contractility and passive stiffness
489 in the main text of this study, respectively. They are input parameters of the model and are not
490 the same as the end-systolic and end-diastolic elastance. End-systolic and diastolic elastance
491 can be calculated as pressure/volume at end-systole and end-diastole and are the result of the
492 complex interaction of E_{\max} , E_{\min} , flows and volumes.

493 Myocardial volume adaptation

494 An increase in systolic contractility due to remodeling is a result of an increased number of
495 myocardial fibers or sarcomeres within each fiber. Many fibers and/or sarcomeres imply a
496 larger myocardial mass. Similarly, a chamber with thicker walls and larger myocardial mass
497 (excluding the presence of fibrotic tissue) would be a chamber with increased resistance to
498 myocardial strain (referred to as passive stiffness in the medical literature). Based on the
499 assumptions that systolic contractility and passive stiffness of each cardiac chamber are directly
500 proportional to the amount of cardiac muscle present in the chamber wall, the total myocardial
501 mass was distributed among the four cardiac chambers in proportion to the sum of the passive
502 stiffness and systolic contractility constant. The origin of this assumption is that in simple
503 geometries with constant Young's modulus, a direct relation exists between exerted strain and
504 material thickness, although many confounding factors such as co-existing fibrosis may
505 influence the analysis in real patients. The set myocardial volume was then automatically tuned
506 by the adaptation rules and changed its value from 160 mL to 148 mL, as shown in Table 1 in
507 the main text. Heart rate was 72 min^{-1} for all simulations.

Calculations – weighted mean

During simulation, hemodynamics variables are updated with a frequency of 4 kHz and new values are based both on the latest parameter changes and the previous simulated values in a weighted manner, according to the following running mean equation:

$$x(t + 1) = 0.999 * x(t - 1) + 0.001 * x(t)$$

A stable mean value is usually reached within 30-60 seconds after each change of physiological state of the model, and memory of previous states is therefore lost well in advance of data harvesting.

Sensitivity to wall shear stress and fiber stress

The target FS was 120 mmHg and the target WSS was 0.0025 mmHg. These values were initially chosen of the same order of magnitude as systolic ventricular pressure and measured myocardial stress (systolic stress of $\sim 160,000$ dyn/cm² corresponding to ~ 120 mmHg) (18) and of measured WSS in large arteries (0.3-1.3 Pa, corresponding to 0.0023-0.0098 mmHg) (36). The final target values were then tuned to provide physiological hemodynamics as a starting point for simulations (Table 1A).

We quantitatively assessed the sensitivity of the main hemodynamics variables and LV properties for an increase and decrease of WSS and FS of 20 % in aortic regurgitation with valve minimum area equal to 0.3 cm² corresponding to a regurgitant flow of 66 mL (See Table 1A). The effects of changing target fiber and wall shear stress on left ventricular size and wall thickness was also explored in the full range of aortic regurgitations as seen in Figure 1A. In summary, the remodeling adaptation target values had the largest impact on hemodynamics and ventricular properties in simulations of severe cases of valve disease. Changes in fiber stress target mainly affects wall thickness/wall volumes, while changes in wall shear stress target mainly affects chamber diameter/volumes. Our chosen target values are supported both by the literature, hemodynamic output and the changes in left ventricular properties.

534 Table 1A – Sensitivity of main hemodynamic variables (model output*) to changes in target
535 wall shear stress and fiber stress.

	Systolic arterial pressure	Diastolic arterial pressure	Mean arterial pressure	Cardiac output	LV EDV	LV ESV	LA pressure	RA pressure	LV min diameter	LV wall volume
Fiber stress	%									
+20% (144 mmHg)	+1	+3	+4	+6	+4	+5	-1	-4	+1	-18
-20% (96 mmHg)	+6	+2	+1	+1	-3	-2	+26	-7	-1	+78
Wall shear stress	%									
+20% (0.003 mmHg)	+6	+5	+6	+9	-5	-23	+10	-2	-8	+5
-20% (0.002 mmHg)	-2	-2	-3	-4	+11	+37	+1	-7	+11	+15

536

537 *Simulations were performed for aortic regurgitation with minimum area equal to 0.3 cm² (moderate severity).

538 LV = left ventricle; EDV = end-diastolic volume; ESV = end-systolic volume; LA = left atrium; RA = right atrium.

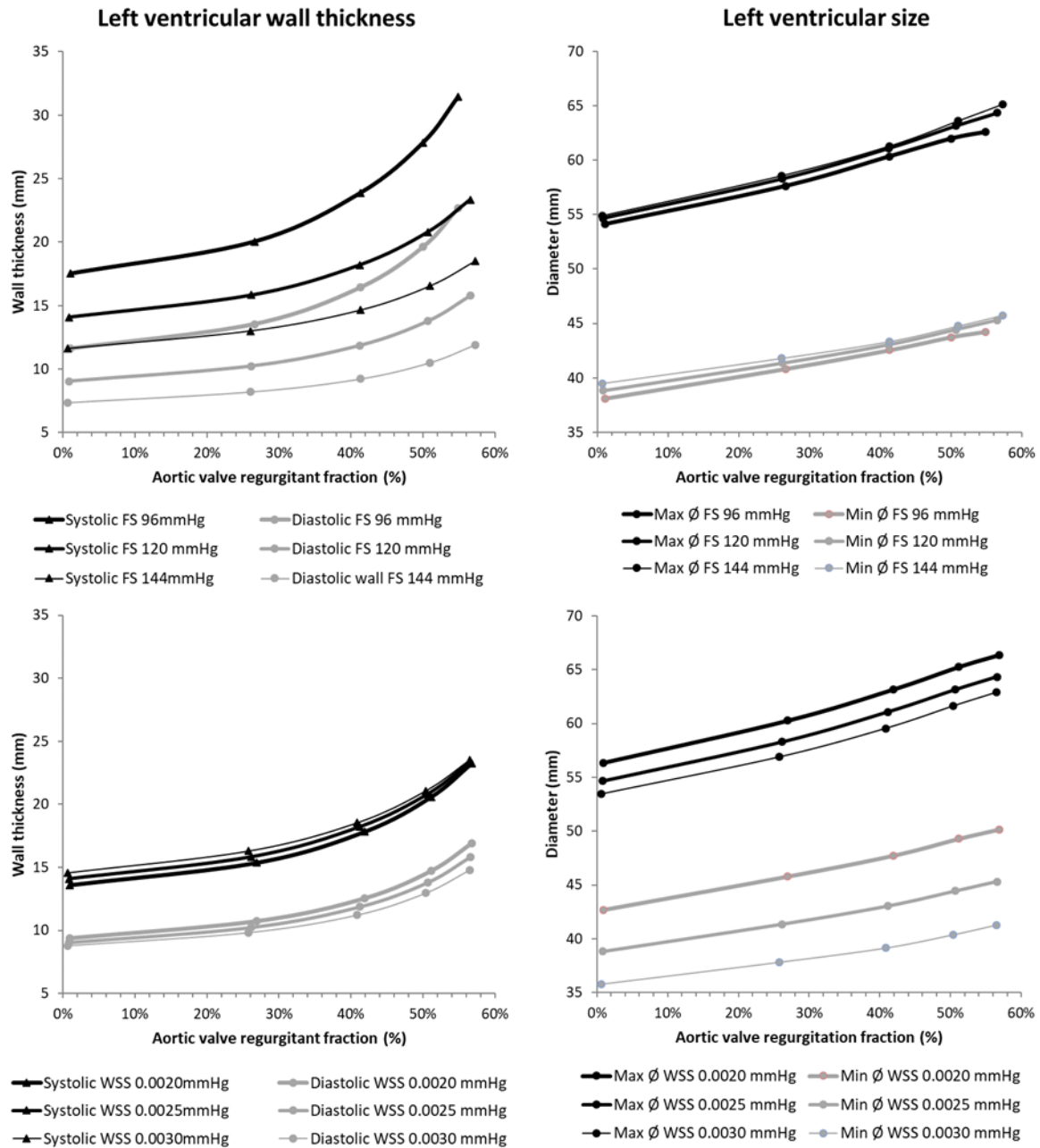


Figure 1A. Sensitivity analysis showing effects of changing target fiber stress and wall shear stress on left ventricular wall thickness and size in aortic regurgitation. A range of regurgitant areas resulting in a regurgitant stroke volume fraction of up to 60% was explored. Changing the target fiber stress influences wall thickness more than ventricular size as shown in the two upper panels. The lower panels show that changing target wall shear stress mainly influences left ventricular size. In general, offsets are more influenced than slopes. Abbreviations: FS; fiber stress, WSS; wall shear stress.

548 **Grants**

549 MBs and EMs research during 2013-2015 was funded by the Swedish Research Council grant
550 2012-2800 and during 2017-2018 by the Stockholm City Council grant SLL20160421. BEW
551 was supported by NWO-VICI (2002406).

552

553 **Disclosures**

554 Michael Broomé is the founder and owner of the company Aplysia Medical AB developing the
555 simulation software Aplysia CardioVascular Lab. There are no other conflicts of interest.

556

557 References

- 558 1. **Arts T, Bovendeerd PH, Prinzen FW, and Reneman RS.** Relation between left
559 ventricular cavity pressure and volume and systolic fiber stress and strain in the wall. *Biophys*
560 *J* 59: 93-102, 1991.
- 561 2. **Arts T, Delhaas T, Bovendeerd P, Verbeek X, and Prinzen FW.** Adaptation to
562 mechanical load determines shape and properties of heart and circulation: the CircAdapt model.
563 *American Journal of Physiology Heart and Circulatory Physiology* 288: H1943-H1954, 2005.
- 564 3. **Arts T, Lumens J, Kroon W, and Delhaas T.** Control of whole heart geometry
565 by intramyocardial mechano-feedback: a model study. *PLoS Comput Biol* 8: e1002369, 2012.
- 566 4. **Arvidsson PM, Kovacs SJ, Toger J, Borgquist R, Heiberg E, Carlsson M, and**
567 **Arheden H.** Vortex ring behavior provides the epigenetic blueprint for the human heart. *Sci*
568 *Rep* 6: 22021, 2016.
- 569 5. **Azevedo PS, Polegato BF, Minicucci MF, Paiva SA, and Zornoff LA.** Cardiac
570 Remodeling: Concepts, Clinical Impact, Pathophysiological Mechanisms and Pharmacologic
571 Treatment. *Arq Bras Cardiol* 106: 62-69, 2016.
- 572 6. **Badiani S, van Zalen J, Treibel TA, Bhattacharyya S, Moon JC, and Lloyd**
573 **G.** Aortic Stenosis, a Left Ventricular Disease: Insights from Advanced Imaging. *Curr Cardiol*
574 *Rep* 18: 80, 2016.
- 575 7. **Broome M, and Donker DW.** Individualized real-time clinical decision support
576 to monitor cardiac loading during venoarterial ECMO. *Journal of translational medicine* 14: 4,
577 2016.
- 578 8. **Broome M, Maksuti E, Bjallmark A, Freckner B, and Janerot-Sjoberg B.**
579 Closed-loop real-time simulation model of hemodynamics and oxygen transport in the
580 cardiovascular system. *Biomedical Engineering Online* 12: 69, 2013.
- 581 9. **Burchfield JS, Xie M, and Hill JA.** Pathological ventricular remodeling:
582 mechanisms: part 1 of 2. *Circulation* 128: 388-400, 2013.
- 583 10. **Chnafa C, Mendez S, and Nicoud F.** Image-based large-eddy simulation in a
584 realistic left heart. *Computers & Fluids* 94: 173-187, 2014.
- 585 11. **Coffey S, Cairns BJ, and Iung B.** The modern epidemiology of heart valve
586 disease. *Heart* 102: 75-85, 2016.
- 587 12. **Cohn JN, Ferrari R, and Sharpe N.** Cardiac remodeling--concepts and clinical
588 implications: a consensus paper from an international forum on cardiac remodeling. Behalf of
589 an International Forum on Cardiac Remodeling. *J Am Coll Cardiol* 35: 569-582, 2000.
- 590 13. **Donker DW, Brodie D, Henriques JPS, and Broome M.** Left Ventricular
591 Unloading During Veno-Arterial ECMO: A Simulation Study. *ASAIO J* 2018.
- 592 14. **Dweck MR, Joshi S, Murigu T, Gulati A, Alpendurada F, Jabbour A,**
593 **Maceira A, Roussin I, Northridge DB, Kilner PJ, Cook SA, Boon NA, Pepper J,**
594 **Mohiaddin RH, Newby DE, Pennell DJ, and Prasad SK.** Left ventricular remodeling and
595 hypertrophy in patients with aortic stenosis: insights from cardiovascular magnetic resonance.
596 *J Cardiovasc Magn Reson* 14: 50, 2012.
- 597 15. **El Sabbagh A, Reddy YNV, and Nishimura RA.** Mitral Valve Regurgitation in
598 the Contemporary Era: Insights Into Diagnosis, Management, and Future Directions. *JACC*
599 *Cardiovasc Imaging* 11: 628-643, 2018.
- 600 16. **Gardner BI, Bingham SE, Allen MR, Blatter DD, and Anderson JL.** Cardiac
601 magnetic resonance versus transthoracic echocardiography for the assessment of cardiac
602 volumes and regional function after myocardial infarction: an intrasubject comparison using
603 simultaneous intrasubject recordings. *Cardiovasc Ultrasound* 7: 38, 2009.
- 604 17. **Genet M, Lee LC, Nguyen R, Haraldsson H, Acevedo-Bolton G, Zhang Z, Ge**
605 **L, Ordovas K, Kozerke S, and Guccione JM.** Distribution of normal human left ventricular

myofiber stress at end diastole and end systole: a target for in silico design of heart failure treatments. *J Appl Physiol* (1985) 117: 142-152, 2014.

18. **Grossman W, Jones D, and McLaurin LP.** Wall stress and patterns of hypertrophy in the human left ventricle. *J Clin Invest* 56: 56-64, 1975.

19. **Gulsin GS, Singh A, and McCann GP.** Cardiovascular magnetic resonance in the evaluation of heart valve disease. *BMC Med Imaging* 17: 67, 2017.

20. **Hill JA, and Olson EN.** Cardiac plasticity. *N Engl J Med* 358: 1370-1380, 2008.

21. **Iung B, Baron G, Butchart EG, Delahaye F, Gohlke-Barwolf C, Levang OW, Tornos P, Vanoverschelde JL, Vermeer F, Boersma E, Ravaud P, and Vahanian A.** A prospective survey of patients with valvular heart disease in Europe: The Euro Heart Survey on Valvular Heart Disease. *Eur Heart J* 24: 1231-1243, 2003.

22. **Khalafvand SS, Hung TK, Ng EY, and Zhong L.** Kinematic, Dynamic, and Energy Characteristics of Diastolic Flow in the Left Ventricle. *Comput Math Methods Med* 2015: 701945, 2015.

23. **Konstam MA, Kramer DG, Patel AR, Maron MS, and Udelson JE.** Left ventricular remodeling in heart failure: current concepts in clinical significance and assessment. *JACC Cardiovasc Imaging* 4: 98-108, 2011.

24. **Kubis N, Checoury A, Tedgui A, and Levy BI.** Adaptive common carotid arteries remodeling after unilateral internal carotid artery occlusion in adult patients. *Cardiovascular Research* 50: 597-602, 2001.

25. **Lee LC, Wenk JF, Zhong L, Klepach D, Zhang Z, Ge L, Ratcliffe MB, Zohdi TI, Hsu E, Navia JL, Kassab GS, and Guccione JM.** Analysis of patient-specific surgical ventricular restoration: importance of an ellipsoidal left ventricular geometry for diastolic and systolic function. *J Appl Physiol* (1985) 115: 136-144, 2013.

26. **Lu D, and Kassab GS.** Role of shear stress and stretch in vascular mechanobiology. *J R Soc Interface* 8: 1379-1385, 2011.

27. **Maksuti E, Westerhof N, Westerhof BE, Broome M, and Stergiopulos N.** Contribution of the Arterial System and the Heart to Blood Pressure during Normal Aging - A Simulation Study. *PLoS One* 11: e0157493, 2016.

28. **Marciniak A, Glover K, and Sharma R.** Cohort profile: prevalence of valvular heart disease in community patients with suspected heart failure in UK. *BMJ Open* 7: e012240, 2017.

29. **McCormick ME, Manduchi E, Witschey WR, Gorman RC, Gorman JH, 3rd, Jiang YZ, Stoeckert CJ, Jr., Barker AJ, Markl M, and Davies PF.** Integrated Regional Cardiac Hemodynamic Imaging and RNA Sequencing Reveal Corresponding Heterogeneity of Ventricular Wall Shear Stress and Endocardial Transcriptome. *J Am Heart Assoc* 5: e003170, 2016.

30. **McMullen JR, and Jennings GL.** Differences between pathological and physiological cardiac hypertrophy: novel therapeutic strategies to treat heart failure. *Clin Exp Pharmacol Physiol* 34: 255-262, 2007.

31. **Mynard JP, Davidson MR, Penny DJ, and Smolich JJ.** A simple versatile model of valve dynamics for use in lumped parameter and one-dimensional cardiovascular models. *International Journal for Numerical Methods in Biomedical Engineering* 28: 626-641, 2011.

32. **Mynard JP, and Smolich JJ.** One-dimensional haemodynamic modeling and wave dynamics in the entire adult circulation. *Ann Biomed Eng* 43: 1443-1460, 2015.

33. **Ozkan A, Kapadia S, Tuzcu M, and Marwick TH.** Assessment of left ventricular function in aortic stenosis. *Nature reviews Cardiology* 8: 494-501, 2011.

34. **Palau-Caballero G, Walmsley J, Gorcsan J, 3rd, Lumens J, and Delhaas T.** Abnormal Ventricular and Aortic Wall Properties Can Cause Inconsistencies in Grading Aortic

Regurgitation Severity: A Computer Simulation Study. *J Am Soc Echocardiogr* 29: 1122-1130 e1124, 2016.

35. **Papaioannou TG, and Stefanadis C.** Vascular wall shear stress: basic principles and methods. *Hellenic J Cardiol* 46: 9-15, 2005.

36. **Reneman RS, Arts T, and Hoeks AP.** Wall shear stress--an important determinant of endothelial cell function and structure--in the arterial system in vivo. Discrepancies with theory. *J Vasc Res* 43: 251-269, 2006.

37. **Rieck AE, Cramariuc D, Boman K, Gohlke-Barwolf C, Staal EM, Lonnebakken MT, Rossebo AB, and Gerdtts E.** Hypertension in aortic stenosis: implications for left ventricular structure and cardiovascular events. *Hypertension* 60: 90-97, 2012.

38. **Ruwhof C, and van der Laarse A.** Mechanical stress-induced cardiac hypertrophy: mechanisms and signal transduction pathways. *Cardiovasc Res* 47: 23-37, 2000.

39. **Schirone L, Forte M, Palmerio S, Yee D, Nocella C, Angelini F, Pagano F, Schiavon S, Bordin A, Carrizzo A, Vecchione C, Valenti V, Chimenti I, De Falco E, Sciarretta S, and Frati G.** A Review of the Molecular Mechanisms Underlying the Development and Progression of Cardiac Remodeling. *Oxid Med Cell Longev* 2017: 3920195, 2017.

40. **Selvetella G, Hirsch E, Notte A, Tarone G, and Lembo G.** Adaptive and maladaptive hypertrophic pathways: points of convergence and divergence. *Cardiovasc Res* 63: 373-380, 2004.

41. **Shabetai R.** Pericardial effusion: haemodynamic spectrum. *Heart* 90: 255-256, 2004.

42. **Shimizu I, and Minamino T.** Physiological and pathological cardiac hypertrophy. *J Mol Cell Cardiol* 97: 245-262, 2016.

43. **Silber HA, Bluemke DA, Ouyang P, Du YP, Post WS, and Lima JA.** The relationship between vascular wall shear stress and flow-mediated dilation: endothelial function assessed by phase-contrast magnetic resonance angiography. *J Am Coll Cardiol* 38: 1859-1865, 2001.

44. **Stokke TM, Hasselberg NE, Smedsrud MK, Sarvari SI, Haugaa KH, Smiseth OA, Edvardsen T, and Remme EW.** Geometry as a Confounder When Assessing Ventricular Systolic Function: Comparison Between Ejection Fraction and Strain. *J Am Coll Cardiol* 70: 942-954, 2017.

45. **Stoylen A, Molmen HE, and Dalen H.** Importance of length and external diameter in left ventricular geometry. Normal values from the HUNT Study. *Open Heart* 3: e000465, 2016.

46. **Treibel TA, Kozor R, Menacho K, Castelletti S, Bulluck H, Rosmini S, Nordin S, Maestrini V, Fontana M, and Moon JC.** Left Ventricular Hypertrophy Revisited: Cell and Matrix Expansion Have Disease-Specific Relationships. *Circulation* 136: 2519-2521, 2017.

47. **Uretsky S, Supariwala A, Nidadovolu P, Khokhar SS, Comeau C, Shubayev O, Campanile F, and Wolff SD.** Quantification of left ventricular remodeling in response to isolated aortic or mitral regurgitation. *J Cardiovasc Magn Reson* 12: 32, 2010.

48. **Wilson AJ, Schoenauer R, Ehler E, Agarkova I, and Bennett PM.** Cardiomyocyte growth and sarcomerogenesis at the intercalated disc. *Cell Mol Life Sci* 71: 165-181, 2014.

49. **Xie M, Burchfield JS, and Hill JA.** Pathological ventricular remodeling: therapies: part 2 of 2. *Circulation* 128: 1021-1030, 2013.

50. **Zarins CK, Zatina MA, Giddens DP, Ku DN, and Glagov S.** Shear stress regulation of artery lumen diameter in experimental atherogenesis. *J Vasc Surg* 5: 413-420, 1987.

706 51. **Zile MR, Baicu CF, and Gaasch WH.** Diastolic heart failure--abnormalities in
707 active relaxation and passive stiffness of the left ventricle. *N Engl J Med* 350: 1953-1959, 2004.
708

Legends

Figure 1. (A) Atria. Both the left and right atrium are approximated to be spheres with an inner radius of r , a wall thickness of h , an inner blood volume of v and a wall volume of v_{wall} . (B) Left ventricle. The left ventricle is approximated to be a half ellipsoid with max inner radius r , wall thickness h and a length of $3r$. (C) Right ventricle. The right ventricle is approximated to be a quarter ellipsoid with max inner radius r , wall thickness h and a length of $3r$.

Figure 2. Simulation output of changes in left ventricular end-diastolic volumes and wall volumes in valvular disease with varying valve areas. Aortic stenosis (AS), mitral regurgitation (MR) and aortic regurgitation (AR). Valve areas for each simulation step are indicated in the figure. AS result in concentric hypertrophy and AR and MR in eccentric hypertrophy (more pronounced hypertrophy in AR).

Figure 3. Simulation output of different degrees of severity of aortic stenosis with myocardial remodeling. A small aortic opening area results in a large increase in systolic and diastolic wall thickness, left ventricular wall volume and a slight decrease in chamber diameter.

Figure 4. Simulation output of different degrees of severity of mitral regurgitation with myocardial remodeling.

Figure 5. Comparison between simulation output in mitral regurgitation and clinical data from Uretsky et al. (47). The linear regression equations are shown in the lower part of each panel.

Figure 6. Simulation output of different degrees of severity of aortic regurgitation with complete myocardial remodeling based on both fiber stress and wall shear stress in the upper row. The middle row shows adaptation of fiber stress excluding adaptation of wall shear stress and the bottom row adaptation of wall shear stress excluding adaptation of fiber stress. Wall shear stress induced dilatation and wall thinning occurs in the bottom row, while wall volume increase with wall thickening occurs in the middle row with only fiber stress adaptation. Both mechanisms are needed for a realistic adaptive remodeling process as seen in the upper row.

Figure 7. Comparison between simulation output in aortic regurgitation and clinical data from Uretsky et al. (47). The linear regression equations are shown in the lower part of each panel.

Figure 8. Measures of systolic function in simulated remodeled aortic stenosis. Ejection fraction (black) is preserved, while elastance (gray) increases with valve stenosis severity. Myofiber shortening (strain) (dashed black) decreases with valve narrowing and increasing hypertrophy.

Table 1. Start values representing normal physiology at mean wall shear stress 0.0025 mmHg and mean myofiber stress 120 mmHg in all chambers. Gray columns show baseline elastance values and white columns chamber dimensions derived from elastance values using the geometric assumptions and remodeling algorithms described in the main text.

Table 2. – Main hemodynamic variables (simulation output) for the normal case and three different degrees of severity of valve diseases.

Figure 1A. Sensitivity analysis showing effects of changing target fiber stress and wall shear stress on left ventricular wall thickness and size in aortic regurgitation. A range of regurgitant areas resulting in a regurgitant stroke volume fraction of up to 60% was explored. Changing the target fiber stress influences wall thickness more than ventricular size as shown in the two upper panels. The lower panels show that changing target wall shear stress mainly influences left ventricular size. In general, offsets are more influenced than slopes. Abbreviations: FS; fiber stress, WSS; wall shear stress.

Table 1A – Sensitivity of main hemodynamic variables (model output*) to changes in target wall shear stress and fiber stress.